Theor. Appl. Climatol. 80, 37–48 (2005)
DOI 10.1007/s00704-004-0079-y

Theoretical and Applied Climatology
Printed in Austria

[1] Institute of Geographical Sciences and Natural Resources Research CAS, Beijing, China
[2] Utah State University, Logan, Utah, USA
[3] LARSIS, Institute of Remote Sensing Applications, CAS, Beijing, China
[4] London Metropolitan University, London, UK
[5] Tsinghua University, Beijing, China

Air temperature retrieval from remote sensing data based on thermodynamics

Y.-J. Sun[1], J.-F. Wang[1], R.-H. Zhang[1], R. R. Gillies[2], Y. Xue[3,4], and **Y.-C. Bo[5]**

With 5 Figures

Received December 15, 2003; revised March 10, 2004; accepted June 8, 2004
Published online October 14, 2004

Summary

A new approach to retrieving air temperature from land surface temperature is presented. The new method is based on thermodynamics. Two important parameters, namely crop water stress index and aerodynamic resistance, were used to build a quantitative relationship between the land surface temperature and the ambient air temperature. The method was applied using MODIS satellite data for a location situated in the North China Plain. Comparing the measurement values at meteorological stations with air temperature, derived by the method for certain pixels, indicates that derived values can be obtained within an accuracy of 3 °C for more than 80% of data processed. Sensitivity studies also suggest that inaccuracies associated with measurement error in the model variables are also within the 3 °C range.

1. Introduction

Air temperature is becoming increasingly important in spatially explicit landscape, regional, and global models (Collins and Bolstad, 1996). However, the generic source of climate data is the meteorological station, which only provides data at single locations (Hartkamp et al., 1999); this necessitates the use of methodologies to estimate values in-between (i.e. at model grid points). Methodologies generally employed, although not limited to, are the vertical lapse method, regional regression methods and other interpolation methods such as inverse distance weighted averaging (IDWA), thin plate smoothing splines and different forms of kriging (Boyer, 1984; De Beurs, 1998; Hutchinson, 1989; Hutchinson and Corbett, 1995; Ishida and Kawashima, 1993). The vertical lapse method adjusts for the commonly observed decrease in temperature with increasing elevation (Barry, 1992). It is suitable in mountainous areas or where there is complex terrain. Regional regression methods employ a network of temperature measurements and fit polynomial equations as functions of elevation and horizontal coordinates (Russo et al., 1993). However, it should be noted that different interpolation methods often optimize the weights of each sampling point according to different standards. All such aforementioned methods are able to estimate annual, monthly, daily mean or extreme temperatures given sufficient sample points (Bolstad et al., 1998). For example, Burrough and McDonnell (1998) noted that when data were abundant, most interpolation techniques gave similar results.

However, when data were sparse, the underlying assumptions about the variation among sampled points often differed and the choice of interpolation method and parameters then became critical. Often though data may be too sparse to use any of the interpolation methods and so alternate ways to derive spatially representative values of air temperature need to be researched.

Land surface temperature (i.e. radiant or radiometric temperature) can be retrieved from thermal infrared remotely sensed data. (Bhattacharya and Dadhwal, 2003; Coll et al., 2003; Fily et al., 2003; Schroedter et al., 2003; Kustas et al., 2003). It is, however, not an easy task to gain estimates of air temperature from such land surface temperatures. Attempts have been made such as that of Cresswell et al. (1999) who applied an empirical solar zenith angle model to establish a statistical relationship between land surface temperature and air temperature. In this paper, we present a thermodynamics-based method to estimate instantaneous air temperature from land surface temperature derived from remote sensing data. The outline of the paper is as follows: The theory is addressed in Section 2. The method is applied and assessed for a case study that follows in Section 3. Finally, some discussion and conclusions are presented in Section 4.

2. Theory

2.1 Air temperature derivation

Energy and mass are exchanged between the atmosphere and the underlying surface – a vegetation canopy or a land surface without vegetation. The exchange of energy is described by the energy balance budget equation

$$R_n = LE + H + G, \tag{1}$$

where R_n is the net radiation (W/m^2), H is the sensible heat flux (W/m^2), LE is the latent heat flux (W/m^2) and G is the soil heat flux (W/m^2). The computation of each item in Eq. (1) is as follows:

LE is the transport of water vapor from the surface (e.g. the vegetation) to the atmosphere. The equation is (Monteith, 1973)

$$LE = \frac{\rho C_p}{\gamma r_a}(e_0 - e), \tag{2}$$

here, e_0 is the vapor pressure of the vegetation canopy (hPa), e is the vapor pressure of the atmosphere above (hPa), ρ is the air density (kg/m^3), C_p is air specific heat at constant pressure ($1004\,J/kg/K$), γ is the psychrometric constant and r_a is the aerodynamic resistance (s/m) term. An alternate expression of formula (2) is given by Zhang (1996)

$$LE = \frac{\rho C_p \Delta}{\gamma r_a}\left[(T_0 - T_a) + \frac{d - d_0}{\Delta}\right], \tag{3}$$

in which Δ is the coefficient of the saturation vapor pressure curve when the temperature of the vegetation canopy and atmosphere is equal to the average temperature (hPa/K), T_0 is the surface temperature (K), T_a is the ambient air temperature (K), d is the air saturation deficiency 1m above the vegetation canopy (hPa) and d_0 is the air saturation deficiency above the vegetation canopy (hPa).

H is the rate of heat loss to the air by convection and conduction, due to the temperature difference. The equation is (Monteith, 1973)

$$H = \rho C_p (T_0 - T_a)/r_a, \tag{4}$$

where, terms are defined previously in Eqs. (2) and (3).

According to Idso et al. (1997), G can be parameterized as a linear function of net radiation, namely

$$G \approx \xi R_n, \tag{5}$$

where, ξ is a variable related to the vegetation cover fraction and the leaf area index. It is estimated accordingly as:

$$\xi = 0.35 * (1 - f) + 0.05 * f, \tag{6}$$

where, f is vegetation cover fraction as defined in Eq. (7) (Gillies and Carlson, 1995; Gillies et al., 1997)

$$f = \left(\frac{\mathrm{NDVI}_i - \mathrm{NDVI}_{\min}}{\mathrm{NDVI}_{\max} - \mathrm{NDVI}_{\min}}\right)^2, \tag{7}$$

in which $\mathrm{NDVI}_{\max}$ and $\mathrm{NDVI}_{\min}$ are respectively the fully vegetated and the bare soil values of NDVI (Normalized Difference Vegetation Index), NDVI_i is the NDVI value of the i^{th} pixel. Algebraic manipulation of formulas (3), (4) and (5) and substitution into Eq. (1) results in an equation for air temperature as

$$T_a = T_0 - \frac{(1 - \xi)R_n r_a \gamma}{\rho C_p(\gamma + \Delta)} + \frac{d - d_0}{\gamma + \Delta}. \tag{8}$$

Next we make use of the crop water stress index (CWSI) to establish the connection between the land surface temperature and the air tempera-

ture. According to Jackson et al. (1981), we can compute CWSI accordingly:

$$\mathrm{CWSI} = 1 - E_d/E_p, \tag{9}$$

where E_d is the real evapotranspiration, and E_p is the potential evapotranspiration. In the definition of E_p, many factors must be considered, such as wind speed, the highest and lowest temperature in a month, saturation vapor pressure, and real vapor pressure (Shen and Tian, 1998). However, a representation (Zhang et al., 2001; Su et al., 2001) that the difference between the net radiation and the soil heat flux can be regarded as potential evapotranspiration is used here and Eq. (9) is therefore expressed as

$$\mathrm{CWSI} = 1 - \frac{LE}{R_n - G}. \tag{10}$$

Now, by substituting *LE* in Eq. (10) with Eq. (3), we can get an expression for d_0

$$d_0 = d + \Delta(T_0 - T_a) - \frac{\gamma \cdot r_a \cdot (1 - \mathrm{CWSI}) \cdot (R_n - G)}{\rho C_p}, \tag{11}$$

and by rewriting d_0 in formula (8) using Eq. (11), the air temperature can be derived as

$$T_a = T_0 - \frac{(1-\xi)R_n \cdot r_a \cdot \mathrm{CWSI}}{\rho C_p}. \tag{12}$$

2.2 Sensitivity of the model

The sensitivity of the model was analyzed through three variables: T_0, f and R_n, because the other two parameters (CWSI and aerodynamic resistance) are functions of them. Cases with a single variable are too simple, so this paper emphasizes the sensitivity to all three variables. Given each variable the error supposed (represented by the symbol Δ), Eq. (12) should be

$$T_a = T_0 + \Delta T_0 - \frac{(1 - (\xi + \Delta\xi))(R_n + \Delta R_n) \cdot r_a \cdot \mathrm{CWSI}}{\rho C_p}. \tag{13}$$

That is

$$T_a = T_0 - \frac{(1-\xi)R_n \cdot r_a \cdot \mathrm{CWSI}}{\rho C_p} + \Delta T_0 + \frac{[\Delta\xi \cdot R_n - (1-\xi)\Delta R_n] \cdot r_a \cdot \mathrm{CWSI}}{\rho C_p}. \tag{14}$$

Then the error in the result of air temperature is:

$$\Delta T_a = \left[T_0 - \frac{(1-\xi)R_n \cdot r_a \cdot \mathrm{CWSI}}{\rho C_p}\right] + \Delta T_0 + \frac{[\Delta\xi \cdot R_n - (1-\xi)\Delta R_n] \cdot r_a \cdot \mathrm{CWSI}}{\rho C_p} - T_{\mathrm{atrue}}, \tag{15}$$

where, T_{atrue} is the ture value of air temperature.

3. Case study

3.1 Study site location

The study area was located in the North China Plane, bounded by latitudes 35° to 38° N and longitudes 114° to 123° E (*ref.*, Fig. 1). The region included some parts of Shandong, Jiangsu, Hebei, Henan and Anhui provinces.

3.2 Input data computation and derivation

The data required as input to Eq. (12) was primarily derived from satellite, in particular the MODIS (moderate resolution imaging spectroradiometer) sensor. Two overpass dates were chosen (April 2nd and July 15th 2002) as a test bed for the method from which early morning and late afternoon images were acquired, processed and utilized in Eq. (12) to derive spatial fields of air temperature. Other data resources comprised land use map data and meteorological data. The components of Eq. (12) are now discussed in more detail.

3.2.1 Land surface temperature

The initial images of land surface temperature, at a resolution of 1 km, were downloaded from NASA's website on the Internet. Land surface temperature was computed from the MODIS image according to the day/night LST algorithm that accounts for surface emissivity (Wan and Li, 1997; Wan, 1999). The LST algorithm has been validated by MAS (MODIS Airborne Simulator) data and field measurement data acquired in field campaigns conducted in 1996–1998 (Wan et al., 1998). To further corroborate the remotely sensed values of land surface temperature, long-term measurement points were taken at Dongping Lake, Shandong province. With the exception

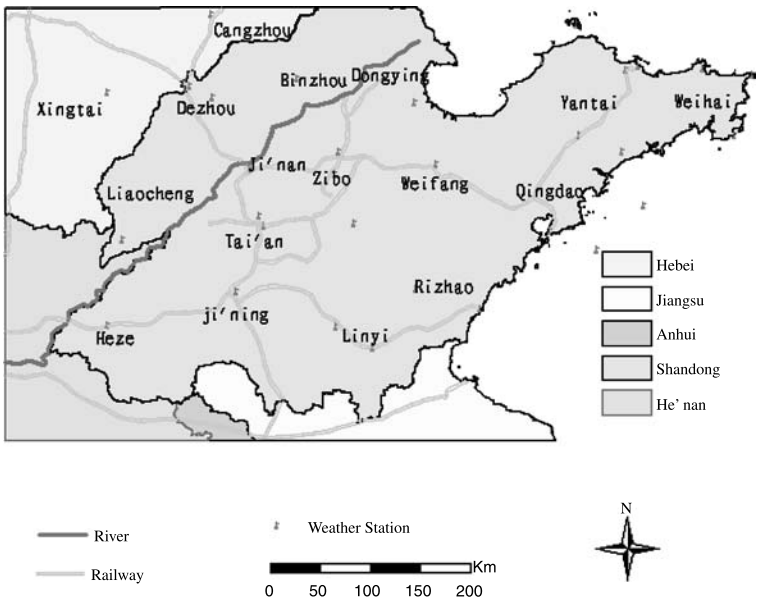

Fig. 1. Site map showing the provinces that encompass the study area

of cloudy and rainy days, measurements were taken twice a day at several points over an area of 1 km^2, i.e. equivalent to a MODIS pixel. One set of measurements were taken before sunrise when the net radiation on the water surface equaled zero while the other set were taken at the time when the MODIS satellite passed over the study area in the late afternoon, at which time the net radiation would be close to a maximum. The means of these measurements were calculated and used as a basis to calibrate those computed through the NASA algorithm.

3.2.2 The ξ parameter

Using Eqs. (6) and (7), ξ was computed using values of NDVI as derived from the MODIS dataset. The initial images of NDVI, at a resolution of 1 km, were downloaded from NASA's website on the Internet. NDVI was computed according to the method described in Huete et al. (1999).

3.2.3 Net radiation

The net radiation was computed according to the following equation (Zhang, 1996)

$$R_n = (1-\rho)S_0 - \sigma\varepsilon_s {T_s}^4 + \sigma\bar{\varepsilon}_a {T_{\text{sky}}}^4 - \sigma(1-\varepsilon_s){T_{\text{sky}}}^4. \quad (16)$$

In Eq. (16) S_0 represents the incoming shortwave radiation from the Sun (W/m^2), ρ is the surface albedo, T_s and T_{sky} are, respectively, the absolute temperatures of the land surface and the sky (K), and ε_s and ε_a are, respectively, the emissivities of the land surface and the atmosphere where the over-bar represents an averaged quantity. σ is the Stefan-Boltzmann constant (5.6697×10^{-8} W m^{-2} K^{-4}). S_0 was measured with a pyrheliograph and supplemented with localized calculations for clear sky conditions. The sky temperature was measured by an infrared thermodetector, with a zenith angle setting of 53°. In addition, an integrated method was used to validate the result. This involved using an instrument that rotated automatically to scan air temperature at different azimuth and zenith angles; results were numerically summed to obtain an integrated temperature. Details of the two methods are to be found in Zhang (1996). Albedo was computed by applying the model of Liang (2001a, b). Emissivities were first measured directly above different land use types to produce a look up table, and then using a land use map for the area, a pixel's emissivity was determined (Zhang et al., 2003) by reference to this look up table. Validation of R_n was carried out at the Yu Cheng Integrated Agricultural Experimental Station, CAS (Chinese Academy of Science). All parameters used in the computation of R_n were measured during the satellite overpass period over the study area. Any errors associated with a time lag in measurement will be addressed in the discussion of the model's sensitivity.

3.2.4 Aerodynamic resistance

The SEBAL (Surface Energy Balance Algorithms for Land) model was used in the computation of aerodynamic resistance (Bastiaanssen et al., 1998a, b; Bastiaanssen, 2000; Pan, 2003). Remotely sensed land surface temperature (Section 3.2.1) can be used in an inversion procedure of the SEBAL model to estimate surface parameters at the regional scale. The advantage of the SEBAL model is in the simplicity of the input parameters together with relatively minor computational overhead. The aerodynamic roughness is the key to the determination of aerodynamic resistance, values of which were assigned according to land use type for each pixel using a prescribed look-up table. The methodology used to determine the aerodynamic resistances is described in the SEBAL training manual (Waters et al., 2002). It involves defining two points, namely a "cold point" and "hot point", which are chosen as boundary conditions in an iteration process whereupon the SEBAL model eliminates the so-called buoyancy effects until the aerodynamic resistance value of the two points become stable. Tables 1 and 2 indicate the parameters used in the iterative process to derive aerodynamic resistance for the MODIS images of April 2nd and July 15th, 2002.

Table 1. Parameters of the iterative process of MODIS image (April 2nd, 2002). Columns labeled *a* and *b* are linear coefficients in the relationship of land surface temperature and air temperature assumed in iteration

Times of iteration	*a*	*b*	r_a (cold) (s/m)	r_a (hot) (s/m)
1	0.448	−131.988	36.576	41.140
2	0.216	−63.413	25.045	21.486
3	0.289	−84.811	28.939	27.687
4	0.258	−75.761	26.987	24.994
5	0.269	−79.034	27.971	26.032
6	0.265	−77.817	27.796	25.690

Table 2. Same as Table 1 except for July 15th, 2002

Times of iteration	*a*	*b*	r_a (cold) (s/m)	r_a (hot) (s/m)
1	0.341	−103.491	33.697	38.261
2	0.167	−50.474	24.803	20.227
3	0.227	−68.775	27.642	26.409
4	0.202	−61.050	26.805	23.867
5	0.211	−63.835	26.602	24.689

3.2.5 CWSI

The difference between all kinds of CWSI's lies in the computation of potential evapotranspiration and thus involves different micrometeorological parameters. In this work, the traditional experimental definition was taken as noted earlier (Eq. (10)); that is, the available energy (R_n-G) is regarded as potential evapotranspiration. To compute potential evapotranspiration, this study adopted the separation method of latent and sensible heat fluxes by Su et al. (2001). In this method, the upper and lower borders formed by the scatter points of apparent thermal inertia

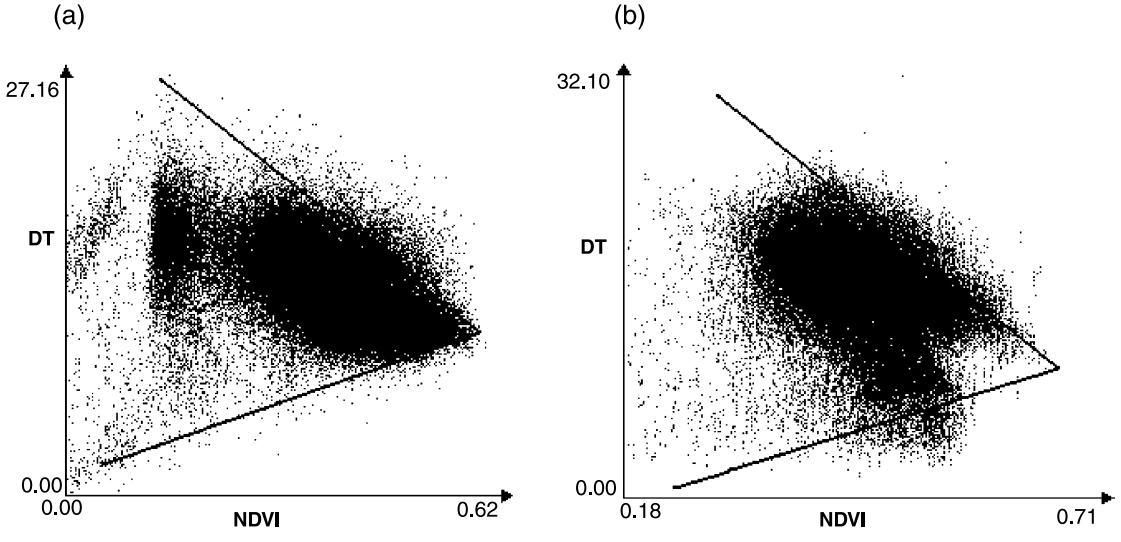

Fig. 2. Scatterplot of apparent thermal inertia versus NDVI for (**a**) April 2nd, 2002, and (**b**) July 15th, 2002

Table 3. Equations of upper border and lower border and Bowen Ratio (April 2nd and July 15th 2002). The terms x and y in the expression of upper border and lower border represents NDVI and DT (apparent thermal inertia) respectively. B represents the Bowen Ratio and the subscript i represents each pixel

	April 2nd	July 15th
Upper Border	$y = -32.3568x + 30.2983$	$y = -46.0905x + 44.6288$
Lower Border	$y = 14.8808x + 1.4598$	$y = 23.9951x - 4.2839$
Bowen Ratio	$B_i = 1 - \frac{32.3568\mathrm{NDVI}_i - 30.2983 + DT_i}{47.2376\mathrm{NDVI}_i - 28.8385}$	$B_i = 1 - \frac{46.0905\mathrm{NDVI}_i - 44.6288 - DT_i}{70.0856\mathrm{NDVI}_i - 48.9127}$

(computed through the land surface temperature difference between day and night MODIS data) and NDVI were identified (*ref.*, Fig. 2). The border equations of each triangle in Fig. 2 are shown in Table 3. Subsequently the Bowen Ratio of each pixel was computed according to the following method (Eq. 17) from Su et al. (2001):

$$B_i = 1 - \frac{DT_u(\mathrm{NDVI}_i) - DT_i}{DT_u(\mathrm{NDVI}_i) - DT_l(\mathrm{NDVI}_i)}. \qquad (17)$$

Here, $DT_u(\mathrm{NDVI}_i)$ represents the upper border of the triangle in Fig. 2, and $DT_l(\mathrm{NDVI}_i)$ represents the lower border of the triangle in Fig. 2. Both are functions of NDVI in each pixel. DT_i is the apparent thermal inertia for each pixel. Lastly, latent and sensible heat fluxes from $(R_n - G)$ were separated according to Eqs. (18) and (19). Whereupon CWSI's of each pixel were computed according to Eq. (10).

$$H_i = (Rn_i - G_i) * \frac{B_i}{1 + B_i}, \qquad (18)$$

$$LE_i = \frac{(Rn_i - G_i)}{1 + B_i}. \qquad (19)$$

Here, H, LE and G are the same as items in Eq. (1).

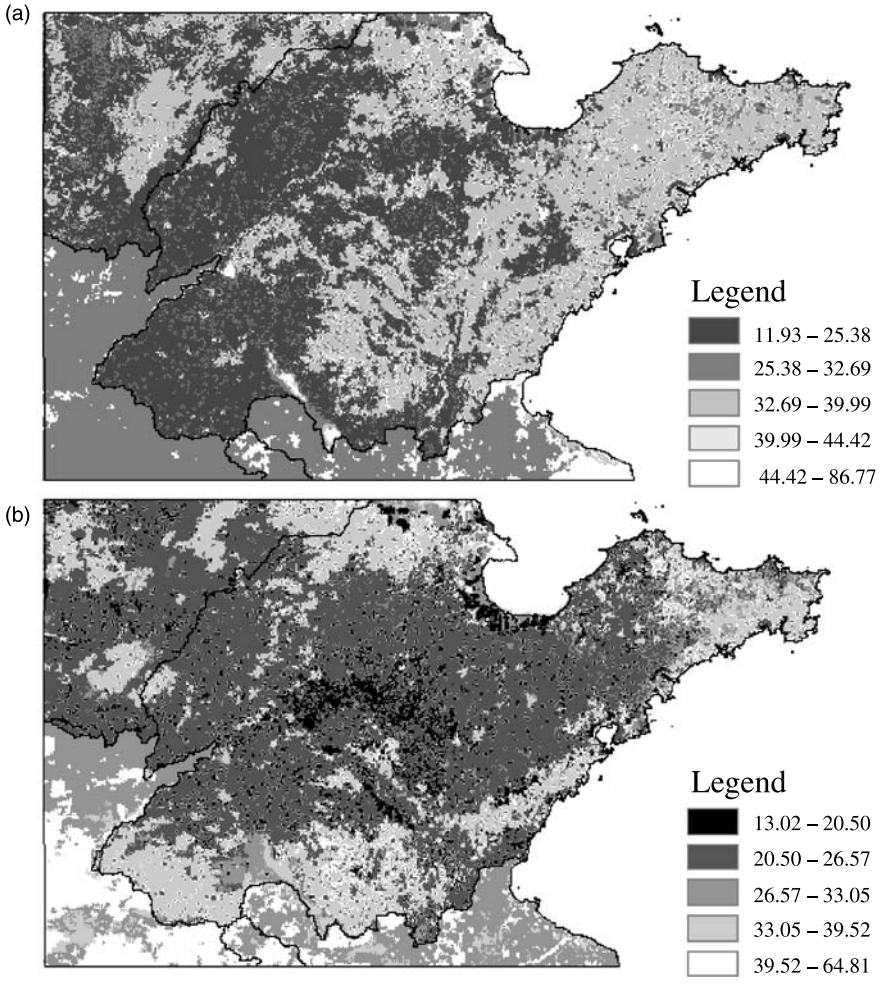

Fig. 3. Aerodynamic resistances derived from MODIS image for (**a**) April 2nd, 2002, and (**b**) July 15th, 2002

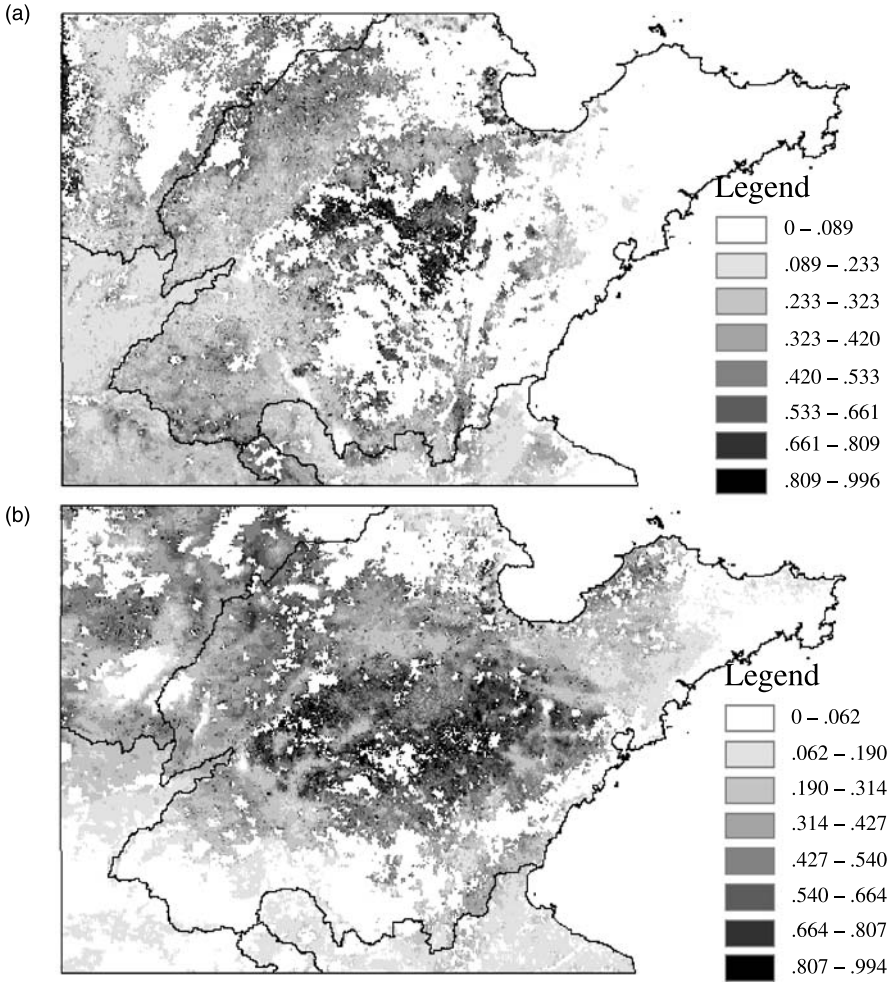

Fig. 4. CWSI derived from MODIS image for (**a**) April 2nd, 2002, and (**b**) July 15th, 2002

3.3 Results and in-situ comparison/ validation

Figure 3 (a and b) shows the inverted result of aerodynamic resistance. Similarly, the CWSI images derived from the separation method of the latent heat flux and the sensible heat flux are shown in Fig. 4 (a and b). Finally by coupling the measurements of land surface temperature, net radiation, derived aerodynamic resistance and CWSI and applying Eq. (12), a spatially derived air temperature map is arrived at the moment of the MODIS satellite overpass for the study area, this is shown in Fig. 5 (a and b).

The results were validated against measurements from standard meteorological stations. There were 33 available weather stations in the study area at the time. As the model required the input of several variables, such as land surface temperature, net radiation and NDVI, all the input data must exist for each pixel to obtain the resultant image of air temperature. If any of the input variables were null for some reason (e.g. cloud covered) then the result was set to zero. Fortunately, at least five pixels corresponding to weather station locations could be used on any particular day. The results of each set of paired data are given in Tables 4 and 5 for both dates. The deviation on April 2nd range from 0.18 to 1.9 °C, and from 0.3 to 3.61 °C on July 15th. An accuracy of about 3 °C was achieved at more than 80% of locations processed.

3.4 Model sensitivity

Data for July 15th were used to examine the sensitivity of the model. Tables 6 through 9 show the deviations in the air temperature computed after perturbing T_0, f and R_n from their initial values individually and jointly. Of note is the fact that the deviation in air temperature

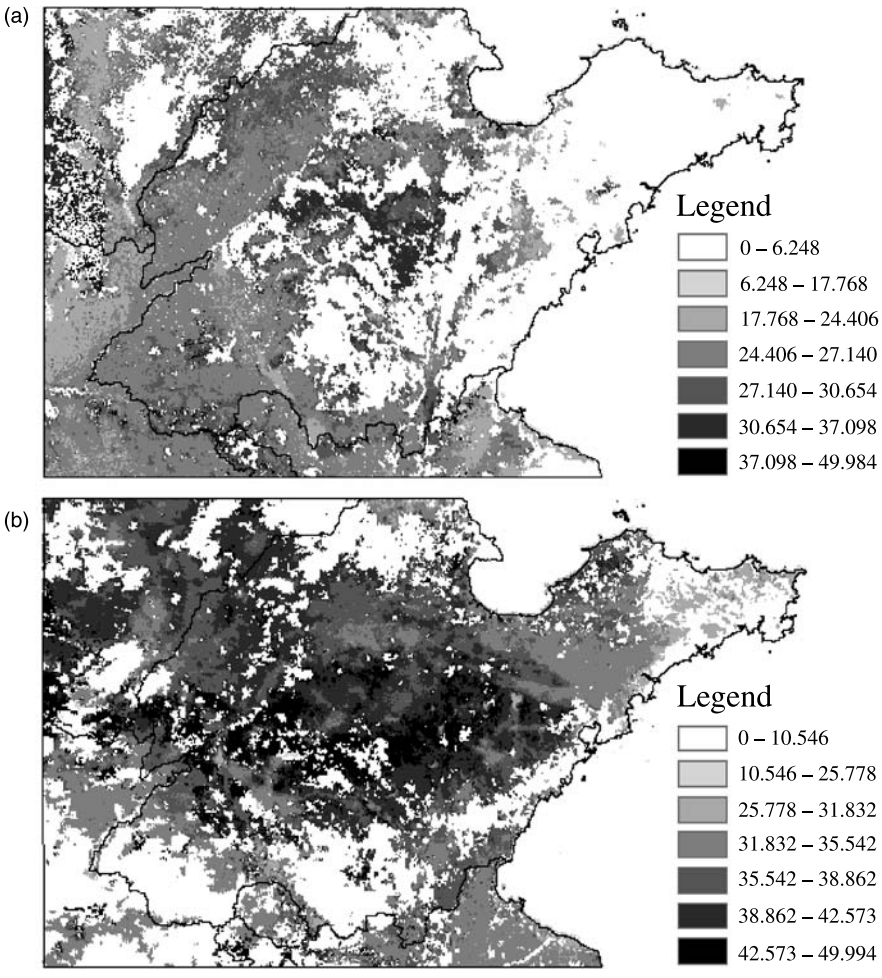

Fig. 5. Air temperature (°C) derived from MODIS image for (**a**) April 2nd, 2002, and (**b**) July 15th, 2002

Table 4. Comparison of air temperature between field measurements and the result inverted from MODIS image (April 2nd, 2002)

ID of weather station	Name of weather station	Measurement value °C	Inversion result °C	Deviation °C
54725	Hui Min	28.7	28.80	0.1
54736	Yang Jiaogou	28.3	29.54	1.24
54705	Nan Gong	29.2	27.93	−1.27
54909	Ding Tao	28.7	27.07	−1.63
54936	Ju Xian	27.2	28.94	1.74

Table 5. Comparison of air temperature between field measurements and the result inverted from MODIS image (July 15th, 2002)

ID of weather station	Name of weather station	Measurement value °C	Inversion result °C	Deviation °C
54725	Hui Min	39.9	40.56	0.66
54705	Nan Gong	41.5	40.73	−0.77
54736	Yang Jiaogou	37.6	41.02	3.42
54824	Zi Chuan	40.0	42.20	2.20
54808	Chao Yang	40.2	38.53	−1.67
54916	Yan Zhou	39.7	36.61	−3.09

Table 6. Deviation of air temperature between field measurements and the result inverted from MODIS image affected by T_0 (July 15th, 2002). P represents ''point''. 6 points were used to verify the sensitivity of the model

ΔT_0 °C	Deviation (°C)					
	P1	P2	P3	P4	P5	P6
1	1.6570	0.2293	4.4177	3.2022	−0.6697	−2.0899
2	2.6570	1.2293	5.4177	4.2022	0.3303	−1.0899
0	0.6570	−0.7707	3.4177	2.2022	−1.6697	−3.0899
−1	−0.3430	−1.7707	2.4177	1.2022	−2.6697	−4.0899
−2	−1.3430	−2.7707	1.4177	0.2022	−3.6697	−5.0899
Ref. of T_a (°C)	39.9	41.5	37.6	40	40.2	39.7

Table 7. Deviation of air temperature between field measurements and the result inverted from MODIS image affected by f (July 15th, 2002). P is as stated for Table 6

Δf (%)	Deviation (°C)					
	P1	P2	P3	P4	P5	P6
10	0.6516	−0.7779	3.4155	2.1987	−1.6781	−3.1031
15	0.6490	−0.7815	3.4144	2.1970	−1.6823	−3.1098
20	0.6463	−0.7851	3.4133	2.1953	−1.6864	−3.1164
0	0.6570	−0.7707	3.4177	2.2022	−1.6697	−3.0899
−20	0.6678	−0.7562	3.4222	2.2092	−1.6530	−3.0635
−15	0.6651	−0.7598	3.4211	2.2075	−1.6572	−3.0701
−10	0.6624	−0.7634	3.4200	2.2057	−1.6614	−3.0767
Ref. of T_a (°C)	39.9	41.5	37.6	40	40.2	39.7

Table 8. Deviation of air temperature between field measurements and the result inverted from MODIS image affected by R_n (July 15th, 2002). P is as stated for Table 6

ΔR_n (%)	Deviation (°C)					
	P1	P2	P3	P4	P5	P6
10	0.5127	−0.8697	3.3235	2.0285	−1.8127	−3.2949
15	0.4406	−0.9193	3.2764	1.9416	−1.8842	−3.3974
20	0.3684	−0.9688	3.2293	1.8547	−1.9557	−3.4999
0	0.6570	−0.7707	3.4177	2.2022	−1.6697	−3.0899
−20	0.9456	−0.5725	3.6062	2.5498	−1.3838	−2.6799
−15	0.8735	−0.6221	3.5591	2.4629	−1.4553	−2.7824
−10	0.8013	−0.6716	3.5120	2.3760	−1.5268	−2.8849
Ref. of T_a (°C)	39.9	41.5	37.6	40	40.2	39.7

Table 9. Deviation of air temperature between field measurements and the result inverted from MODIS image affected by T_0, f and R_n (July 15th, 2002). P is as stated for Table 6

Δ			Deviation (°C)					
T_0 (°C)	f (%)	R_n (%)	P1	P2	P3	P4	P5	P6
1	10	10	−0.2003	−1.6737	2.5064	1.3773	−2.5287	−3.8918
1.5	15	15	−0.6255	−2.1205	2.0547	0.9659	−2.9530	−4.2827
2	20	20	−1.0507	−2.5674	1.6029	0.5545	−3.3774	−4.6736
0	0	0	0.6570	−0.7707	3.4177	2.2022	−1.6697	−3.0899
−2	−20	−20	2.3507	1.0074	5.2171	3.8455	0.0174	−1.5464
−1.5	−15	−15	1.9255	0.5605	4.7653	3.4341	−0.4070	−1.9373
−1	−10	−10	1.5003	0.1137	4.3136	3.0227	−0.8313	−2.3282
Ref. of T_a (°C)			39.9	41.5	37.6	40	40.2	39.7

is of a magnitude and extent similar to the results reported in Section 3.3, this being the case whether the three variables were changed individually or jointly. It also seems not to matter whether they are skewed in the positive or negative direction as this does not cause any significant change in the deviation of derived air temperature, as retrieved from the use of MODIS images, compared with air temperature measured at the meteorological stations. This result indicates that the method of air temperature determination can endure error in the computation of the input within the limits tested here.

4. Conclusions and discussion

In this paper, we suggest a new method (based on thermodynamics) to retrieve regional air temperature using remotely sensed data (MODIS). CWSI was used as the basis for the establishment of the relationship between air temperature and land surface temperature. The method was applied for a region located in the North China Plain. An accuracy of within 3 °C was achieved for more than 80% of the data processed and sensitivity studies also indicate that measurement errors result in similar deviations in air temperature from that observed. The method may be applied to other similar satellite data that have morning and afternoon overpasses (e.g. AVHRR), as the underlying processes based on thermodynamics will remain the same.

The determination of CWSI and aerodynamic resistance are two parameters that are crucial to the method. As for CWSI, different methods can be used to compute it with different sources of data: for example, meteorological data or, more recently, microwave remote sensing data (Seguin et al., 1991; Paloscia and Pampaloni, 1984). In the computation of aerodynamic resistance the difficulty lies in defining the aerodynamic roughness. In the SEBAL model, aerodynamic roughness is determined according to land use type using an experimental look-up table. However, aerodynamic roughness can also be computed based on mechanics (Zhu, 2003), but more data and more complex equations are needed. Moreover, the SEBAL model is a single-layer model that by definition only accounts for single-direction transfer between the land surface and the atmosphere. A more accurate model to compute aerodynamic resistance could include more functionality but may be offset by excess data requirements that may be difficult to obtain with required accuracy. The algorithms used to compute the two parameters in the paper are simple but the results obtained in this study should certainly be of interest to investigators working in areas where there is no adequate data available or where air temperature measurements are sparse. It is envisaged that, with improved methods for computing CWSI and aerodynamic resistance, a better level of accuracy could be achieved.

The resolution of the retrieved air temperature is by definition at 1 km, this being the spatial resolution resolved at the MODIS sensor. The reasons for the comparatives with measurements from the meteorological stations are simply pragmatic, i.e. meteorological stations are the only references that were currently available. The inversion method of air temperature, however, transcends numerous surface types while measurements from the meteorological stations conform to a standard and so stations maintain similar underlying surfaces, i.e. they are generally grassy. It is therefore to be expected that differences will occur as a result of this and while certainly an issue, better representation of the surface at the pixel scale will be addressed in future research. Furthermore, a validation using 5–6 points is not sufficient to statistically assess the accuracy of the method. The new methodology we describe in this paper is an initial trial to retrieve non-remote sensing parameters (i.e. air temperature) by the way of remote sensing (MODIS land surface temperature).

References

Barry RG (1992) Mountain weather and climate, 2nd edn. London: Routledge

Bastiaanssen WGM (2000) SEBAL-based sensible and latent heat fluxes in the irrigated Gediz Basin, Turkey. J Hydrol 229: 87–100

Bastiaanssen WGM, Menenti M, Feddes RA, Holtslag AAM (1998a) A remote sensing surface energy balance algorithm for land (SEBAL): 1 Formulation. J Hydrol 212–213, 198–212

Bastiaanssen WGM, Pelgrum H, Wang J, Ma Y, Moreno JF, Oerink GJ, van der Wal T (1998b) A remote sensing

surface energy balance algorithm for land (SEBAL): 2 Validation. J Hydrol 212: 213–229

Bhattacharya BK, Dadhwal VK (2003) Retrieval and validation of land surface temperature (LST) from NOAA AVHRR thermal images of Gujarat, India. Int J Remote Sensing 24: 1197–1206

Bolstad PV, Swift L, Collins F, Régnière J (1998) Measured and predicted air temperatures at basin to regional scales in the southern Appalachian mountains. Agric Forest Meteorol 91: 161–176

Boyer DG (1984) Estimation of daily temperature means using elevation and latitude in mountainous terrain. Water Resour Bull 4: 583–588

Burrough PA, Mc Donnell RA (1998) Principles of geographical information systems. New York: Oxford University Press

Coll C, Caselles V, Valor E, Rubio E (2003) Validation of temperature-emissivity separation and split-window methods from TIMS data and ground measurements. Remote Sensing Environ 85: 232–242

Collins FC, Bolstad PV (1996) A comparison of spatial interpolation techniques in temperature estimation. In: Proceedings of the Third International Conference/ Workshop on Integrating GIS and Environmental Modeling, Santa Fe, New Mexico, Santa Barbara, California: National Center for Geographic Information Analysis

Cresswell MP, Morse AP, Thomson MC, Connor SJ (1999) Estimating surface air temperatures, from Meteosat land surface temperatures, using an empirical solar zenith angle model. Int J Remote Sensing 20: 1125–1132

De Beurs K (1998) Evaluation of spatial interpolation techniques for climate variables: Case study of Jalisco, Mexico. MSc thesis. Department of Statistics and Department of Soil Science and Geology, Wageningen Agricultural University, The Netherlands

Fily M, Royer A, Goïta K, Prigent C (2003) A simple retrieval method for land surface temperature and fraction of water surface determination from satellite microwave brightness temperatures in sub-arctic areas. Remote Sensing Environ 85: 328–338

Gillies RR, Carlson TN (1995) Thermal remote sensing of surface soil water content with partial vegetation cover for incorporation into climate models. J Appl Meteor 34: 745–756

Gillies RR, Carlson TN, Cui J, Kustas W, Humes K (1997) A verification of the ''triangle'' method for obtaining surface soil water content and energy fluxes from remote measurements of the normalized difference vegetation index (NDVI) and surface radiant temperature. Int J Remote Sensing 18: 3145–3166

Hartkamp AD, De Beurs K, Stein A, White JW (1999) Interpolation techniques for climate variables. NRG-GIS Series 99-01. Mexico, DF: CIMMYT

Huete A, Justice C, Leeuwen W (1999) MODIS VEGETATION INDEX (MOD 13): Algorithm theoretical basis document, version 3.0. http://eospso.gsfc.nasa.gov

Hutchinson MF (1989) A new objective method for spatial interpolation of meteorological variables from irregular networks applied to the estimation of monthly mean solar radiation, temperature, precipitation and windrun. Technical Report 89-5, Division of Water Resources, the Commonwealth Scientific and Industrial Research Organization (CSIRO), Canberra, Australia, pp 95–104

Hutchinson MF, Corbett JD (1995) Spatial interpolation of climate data using thin plate smoothing splines. In: Coordination and harmonization of databases and software for agroclimatic applications. Agroclimatology Working paper Series, 13. Rome: FAO

Idso SB, Jackson RD, Reginator RJ (1997) Remote sensing of crop yields. Science 196: 19–25

Ishida T, Kawashima S (1993) Use of cokriging to estimate surface air temperature from elevation. Theor Appl Climatol 47: 147–157

Jackson RD, Idso SB, Reginato RJ, Pinter PJ (1981) Canopy temperature as a crop water stress indication. Water Resour Research 17: 1133–1138

Kustas WP, Norman JM, Anderson MC, French AN (2003) Estimating subpixel surface temperatures and energy fluxes from the vegetation index-radiometric temperature relationship. Remote Sensing Environ 85: 429–440

Liang S (2001a) Narrowband to Broadband Conversion of Land Surface Albedo. I. Algorithms. Remote Sensing Environ 76: 213–238

Liang S (2001b) Numerical experiments on spatial scaling of land surface albedo and leaf area index. Remote Sensing Reviews 19: 225–242

Monteith JL (1973) Principles of environmental physics. Great Britain: Whitstable Litho Ltd., Whitstable, Kent

Paloscia S, Pampaloni P (1984) Microwave remote sensing of plant water stress. Remote Sensing Environ 16: 249–255

Pan ZQ (2003) Dynamic analysis of evapotranspiration based on remote sensing and GIS in Yellow River Delta of China. PhD thesis of Chinese Academy of Science

Russo JM, Liebhold AM, Kelley JGW (1993) Mesoscale weather data as input to a gypsy moth (Lepidoptera: Lymantriidae) phenology model. J Economic Entomology 86: 838–844

Schroedter M, Olesen F, Fischer H (2003) Determination of land surface temperature distributions from single channel IR measurements: an effective spatial interolation method for the use of TOVS, ECMWF and radiosonde profiles in the atmospheric correction scheme. Int J Remote Sensing 24: 1189–1196

Seguin B, Lagouarde JP, Savane M (1991) The assessment of regional crop water conditions from meteorological satellite thermal infrared data. Remote Sensing Environ 35: 141–148

Shen GR, Tian GL (1998) Drought monitoring with crop water stress index. Agricultural Research in the Arid Areas 16: 123–128

Su HB, Zhang RH, Tang XZ, Sun XM, Zhu ZL, Liu ZM (2001) A simplified method to separate latent and sensible heat fluxes using remotely sensed data. IGARSS (The International Geoscience and Remote Sensing Symposium)

Wan ZM (1999) MODIS Land Surface Temperature Algorithm Theoretical Basis Document (LST ATBD), version 3.3. http://eospso.gsfc.nasa.gov

Wan ZM, Feng YZ, Zhang YL, King MD (1998) Land-surface temperature and emissivity retrieval from MODIS Airborne Simulator (MAS) data. Summaries of the Seventh JPL Airborne Earth Science Workshop 3: 57–66

Wan ZM, Li ZL (1997) A physics-based algorithm for retrieving land-surface emissivity and temperature from EOS/MODOIS Data. IEEE Trans Geosci Remote Sens 35: 980–996

Waters R, Allen R, Tasumi M, Trezza R, Bastiaanssen W (2002) SEBAL-Advanced Training and User Manual

Zhang RH (1996) Experimental remote sensing modeling and surface foundations. Beijing: Sciences Press

Zhang RH, Su HB, Li ZL, Sun XM, Tang XZ, Becker F (2001) The potential information in the temperature difference between shadow and sunlit of surfaces and a new way of retrieving the soil moisture. Science IN China (Series D) 44: 112–123

Zhang RH, Sun XM, Liu JY, Su HB, Tang XZ, Zhu ZL (2003) Determination of regional distribution of crop transpiration and soil water use efficiency using quantitative remote sensing data through inversion. Science IN China (Series D) 46: 10–22

Zhu CY (2003) The retrieval of aerodynamic surface roughness from SAR and TM remote sensing image. PhD thesis of Chinese Academy of Science

Authors' addresses: Yingjun Sun (e-mail: sunyj@lreis.ac.cn or syjldb@hotmail.com) Jinfeng Wang, Renhua Zhang, Institute of Geographical Sciences and Natural Resources Research CAS, Beijing 100101, China; R. R. Gillies, Department of Plants, Soils, and Biometeorology, Department of Aquatic, Watershed and Earth Resources, Utah State University, Logan, Utah 84322-4820, U.S.A.; Yong Xue, LARSIS, Institute of Remote Sensing Applications, Chinese Academy of Sciences, P.O. Box 9718, Beijing 100101, China; Department of Computing, London Metropolitan University, 166-220 Holloway Road, London N7 8DB, UK; Yanchen Bo, Institute of Environmental System Analysis, Department of Environmental Science and Engineering, Tsinghua University, Beijing 100084, China.